Environmental Science & Technology

pubs.acs.org/est

Article

Dissimilatory and Cytoplasmic Antimonate Reductions in a Hydrogen-Based Membrane Biofilm Reactor

Jingzhou Zhou, Chengyang Wu, Si Pang, Lin Yang, Mengying Yao, Xiaodi Li, Siqing Xia,* and Bruce E. Rittmann

Cite This: *Environ. Sci. Technol.* 2022, 56, 14808−14816

Read Online

ACCESS | Metrics & More | Article Recommendations | Supporting Information

ABSTRACT: A hydrogen-based membrane biofilm reactor (H_2-MBfR) was operated to investigate the bioreduction of antimonate [Sb(V)] in terms of Sb(V) removal, the fate of Sb, and the pathways of reduction metabolism. The MBfR achieved up to 80% Sb(V) removal and an Sb(V) removal flux of 0.55 g/m^2·day. Sb(V) was reduced to Sb(III), which mainly formed Sb_2O_3 precipitates in the biofilm matrix, although some Sb(III) was retained intracellularly. High Sb(V) loading caused stress that deteriorated performance that was not recovered when the high Sb(V) loading was removed. The biofilm community consisted of DSbRB (dissimilatory Sb-reduction bacteria), SbRB (Sb-resistant bacteria), and DIRB (dissimilatory iron-reducing bacteria). Dissimilatory antimonate reduction, mediated by the respiratory arsenate reductase ArrAB, was the main reduction route, but respiratory reduction coexisted with cytoplasmic Sb(V)-reduction mediated by arsenate reductase ArsC. Increasing Sb(V) loading caused stress that led to increases in the expression of *arsC* gene and intracellular accumulation of Sb(III). By illuminating the roles of the dissimilatory and cytoplasmic Sb(V) reduction mechanism in the biofilms of the H_2-MBfR, this study reveals that the Sb(V) loading should be controlled to avoid stress that deteriorates Sb(V) reduction.

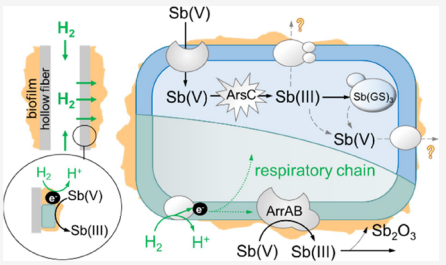

KEYWORDS: *membrane biofilm reactor, antimonate, bioreduction, respiration, toxicity resistance*

INTRODUCTION

Antimony (Sb) is widely used in the semiconductor, battery, textile, and catalyst industries.[1] Antimony has become the ninth most-mined metal in the world, and China accounts for more than 52%.[2] Because of antimony's large industrial production and use, it has become a widespread pollutant in aquatic environments.[3] The European Council, the United States Environmental Protection Agency, the Chinese Environmental Protection Agency, and the Japanese Environmental Protection Agency all classify Sb as a priority pollutant.

At neutral pH, Sb(V) in the form of $Sb(OH)_6^-$ dominates in oxic conditions, while Sb(III) as $Sb(OH)_3$ is more prevalent in anoxic environments.[4] Sb(III) is more toxic than Sb(V), but has lower mobility because $Sb(OH)_3$ precipitates as Sb_2O_3(s).[5,6] Sb(III) also precipitates readily with sulfide or can be strongly adsorbed by Fe(III) hydroxides at neutral pH.[7] In antimony mining and smelting, Sb appears in the surface water as Sb(V) at 0.33−11.4 ppm, while Sb(III) is not detected.[8]

The $Sb(OH)_6^-/Sb(OH)_3$ redox couple has a high potential (760 mV),[9] and previous studies report that respiratory Sb(V) bioreduction can occur during short-term cultivation.[7,10,11] Hence, biologically reducing Sb(V) to Sb(III) is a feasible method for removing Sb from the aqueous phase. Using H_2 as the electron donor for Sb(V) reduction is promising, because H_2 is nontoxic, is relatively inexpensive, leaves no residual organic substrate, and has been applied for microbiological reductions of various oxidized contaminants.[12,13] The stoichiometry and energetics of Sb(V) reduction using H_2 are as follows:

$$Sb(OH)_6^- + H_2 + H^+ = Sb(OH)_3 + 3H_2O$$
$$\Delta G^{0'} = -73.33\ \text{kJ/mol e}^- \quad (1)$$

in which $\Delta G^{0'}$ is the standard free energy adjusted to pH = 7.[14] $\Delta G^{0'}$ has a large negative value, which means that the H_2-based reduction of Sb(V) is energetically favorable.

One challenge for using H_2 as an electron donor is its low water solubility.[15] The challenge is overcome by using the H_2-based membrane biofilm reactor (MBfR), in which H_2 diffuses through the walls of nonporous hollow fiber membranes and is delivered directly to a biofilm attached on the outside surface of the membrane.[16,17] The bacteria oxidize the H_2 and use the electrons to drive microbial respiration of many oxidized contaminants, including antimony.[18] Considering the thermodynamic feasibility of H_2 oxidation and the high H_2-delivery

Received: July 12, 2022
Revised: September 14, 2022
Accepted: September 23, 2022
Published: October 6, 2022

efficiency, the H_2-MBfR is a promising approach for Sb bioremediation.

The current understanding of antimony biochemistry is roughly equivalent to that of arsenic some 20 years ago.[19] Prokaryotes have two arsenate-reduction pathways, dissimilatory and cytoplasmic reductions.[20−22] Dissimilatory antimonate respiration is mediated by a periplasmic arsenate reductase (ArrA),[23,24] while the *ars* operon and arsenate reductase (ArsC) linked to cytoplasmic (non-respiratory) reduction have been observed to increase with Sb(III) exposure.[20,25] ArsC reduces arsenate in the cell's cytoplasm using glutathione (GSH) as the electron donor, and the cells immobilize As(III) or Sb(III) into a vacuole, as glutathione binds $As(GS)_3$ and $Sb(GS)_3$.[26] ArsC may also mediate Sb(V) reduction. Although Sb(V) reduction appears promising for bioremediation, the reduction mechanism is unresolved.[27] It is particularly important to know whether the arsenate-reduction enzymes are responsible for Sb(V) reduction.

We investigated Sb(V) reduction and removal in a H_2-based MBfR. The fate of Sb was analyzed using scanning electron microscopy (SEM), transmission electron microscope (TEM), energy dispersive X-ray spectroscopy (EDS), and X-ray photoelectron spectroscopy (XPS). The pathway of antimonate reduction was analyzed using Illumina sequencing of the 16S rRNA gene, *arrA* gene, and *arsC* gene, along with real-time quantitative Polymerase Chain Reaction/Reverse Transcription-Quantitative Polymerase Chain Reaction (qPCR/RT-qPCR). An antimony-metabolism mechanism is proposed based on our results.

MATERIALS AND METHODS

Reactor Configuration. The MBfR configuration (Figure S1 in the Supporting Information) was similar to our previous work.[28] Briefly, the MBfR included two glass columns: a main column containing a 32-fiber bundle and the biofilm-sampling column with 10 fibers. The hollow fibers were nonporous polypropylene (Teijin, Japan), which ensured bubble-free H_2 delivery to a biofilm that accumulated on the exterior surface. The absolute pressure of H_2 gas was controlled at 1.5 atm during the whole operating period to ensure the sufficient supply of H_2 (0.366 g H_2 m^{-2} d^{-1} according to eq S1 in Table S1[29]). The temperature was maintained at 25 ± 1 °C. More details are listed in Table S1.

Acclimation, Start Up, and Operation. The inoculum was collected from an anaerobic digestor at the Bailonggang Wastewater Treatment Plant (Shanghai, China). It was acclimated with basal salts medium 1 (BSM1, containing phosphate buffer, trace elements, and bicarbonate as inorganic carbon source, detailed in the Supporting Information), 50 mg/L NO_3^--N (supplied daily after deoxygenation with 99.99% N_2 gas), and pure H_2 gas supplied from a gas-tight aluminum foil bag.

To start up the MBfR, 50 mL of sludge that has been acclimated for 7 days was injected into the MBfR, which was then operated in the batch mode for 24 h by recirculating deoxygenated basal salts medium 2 (BSM2, containing bicarbonate as the inorganic carbon source, phosphate buffer, trace elements, detailed in the Supporting Information) containing an initial concentration of 10 mg/L NO_3^-−N.

In Stages 0 to 4 (labeled S0−S4), the MBfR was operated in the continuous-flow mode, with the influent flow rate maintained at 0.29 mL/min. The recirculation rate was 100 mL/min to ensure that the liquid contents of the MBfR were completely mixed.[30]

In S0, the MBfR reactor was fed 10 mg/L NO_3^-−N until the nitrate and nitrite concentrations in the effluent reached the steady state. Subsequently, the MBfR was fed with 5, 10, 30, and 10 mg/L of Sb (provided as $KSb(OH)_6$, AR, Ourchem, China) as the sole electron acceptor without nitrate supply for Stages S1, S2, S3, and S4, respectively. The influent's dissolved oxygen was deoxygenated to below 1 mg/L in BSM2 (details in the Supporting Information). The concentrations in S1 and S2 simulated actual wastewater containing Sb(V), S3 was investigated for the performance with high-loading stress, and S4 was set up to observe the recovery from S3. In each stage, the reactor was considered at the steady state when the effluent concentration of all the substrates and the products had ≤5% variation for at least 3 HRTs.[15]

Chemical Analyses. Ten microliters of effluent samples were filtered through a 0.22 μm membrane filter (25 mm PES, Titan, China) immediately after collection with a syringe every day. The concentrations of Sb(V) were assayed by an anion ion chromatograph (Dionex Aquion, USA) with an AS19 column and AG19 precolumn, an eluent concentration of 15 mM KOH, and a 1 mL/min flow rate. The concentrations of Sb(III) were assayed using high-performance liquid chromatography−inductively coupled plasma−mass spectrometry (HPLC-ICP-MS) (Agilent LC1200-ICPMS 7700, Agilent, USA). The HPLC instrument was equipped with an anion exchange column (PRP-X100, 4.1 × 150 mm, 10 μm, Hamilton, Switzerland). EDTA (20 mM)and 2 mM potassium hydrogen-phthalate at pH 4.5 were applied as the mobile phase, which was delivered at a constant flow rate of 1 mL/min.[31] The water samples were diluted 100-fold with ultrapure water, and the injection volume was 10 μL. The pH of the influent and effluent was measured with a pH meter (HQ1110, HACH, USA). The influent pH was stable at 7.0 ± 0.1, and effluent pH ranged from 7.2 to 7.8.

Flux Calculations. The Sb(V)- and O_2-removal fluxes (g/m^2 d) were calculated according to

$$J = \frac{Q(S_0 - S)}{A} \tag{2}$$

where S_0 and S are the influent and effluent Sb(V) or O_2 concentration (g/L), Q is the influent flow rate to the MBfR (L/d), and A is the membrane surface area (m^2). The H_2 flux in each stage was calculated from the Sb(V)-removal flux and the O_2-removal flux according to reaction stoichiometry based on Rittmann and McCarty:[32]

$$Sb(OH)_6^- + 1.67H_2 + 0.33HCO_3^- + 0.067NH_4^+ = 0.067C_5H_7O_2N + Sb(OH)_3 + 2.6H_2O + 1.27OH^- \tag{3}$$

$$O_2 + 3.33H_2 + 0.667HCO_3^- + 0.133NH_4^+ = 0.133C_5H_7O_2N + 3.197H_2O + 0.533OH^- \tag{4}$$

The maximum possible H_2 flux was computed from Tang et al. based on the lumen's H_2 pressure.[29] The actual H_2 fluxes were calculated from $J_{H_2} = J_{Sb(V)} \times 1.67 \times 2/121.8 + J_{O_2} \times 3.33 \times 2/32$ and always were much smaller than the maximum H_2 delivery flux, which means that the H_2 supply is sufficient over the operation.

https://doi.org/10.1021/acs.est.2c04939
Environ. Sci. Technol. 2022, 56, 14808−14816

Biofilm Sampling, DNA Extraction, and Microbial Community Analysis. Biofilm samples were collected at the end of S1, S2, S3, and S4. Two 18-cm-long sections from a coupon fiber were cut off for DNA extraction and RNA separation. The open end of the remaining fiber was tied with 2 knots to avoid H_2 leakage.

Genomic DNA was extracted with a DNeasy PowerBiofilm Kit (QIAGEN GmbH, Germany) according to the manufacturer's specification. The DNA concentration was measured using NanoDrop 2000 (Thermo Fisher Scientific, USA).

PCR primers 338F and 806R were applied to amplify the V3-V4 region of the bacteria's 16S rRNA gene.[33] The Illumina MiSeq PE300 platform (Majorbio Bio-pharm Technology Co., Ltd., Shanghai, China) was used to sequence the amplicons. Sequence data were analyzed on the online platform of the Majorbio ISanger Cloud Platform. Qualified sequences were clustered into operational taxonomic units (OTUs) at 97% similarity using the Uparse software version 11.[34] Based on the OTU information, the richness and evenness of microbial species were evaluated. The Spearman correlation coefficient ρ of influent Sb(V) and genus abundance was calculated using GraphPad Prism 9.

To further identify key microorganisms carrying out Sb(V) reduction, we amplified the *arrA* gene using primer sets CVF1/CVR1, the *arsC* gene using amlt−42−f/amlt−376−r (Table S2). The amplicons were sent to Majorbio Technology (Shanghai, China) for Illumina functional gene sequencing. Taxonomic analysis was done using the QIIME2 pipeline and NT databases.

RNA Extraction, qPCR, and RT-qPCR. The total RNA was extracted using a TaKaRa MiniBEST Universal RNA Extraction Kit (TaKaRa, Japan), and it was reverse-transcribed to cDNA following the instructions of the PrimeScript RT reagent Kit with the gDNA Eraser (Perfect Real Time, TaKaRa, Japan).[35]

The biological antimony-reduction potential was characterized by the copy numbers and transcription levels of the *arrA* (arsenate respiratory reductase gene) and *arsC* (arsenate reductase gene).

The designed qPCR primer pairs and primer sequences are shown in Table S2. All qPCR/RT-qPCR analyses were performed using the CFX Connect Real-Time PCR System (Bio-Rad, USA). The qPCR/RT-qPCR amplification mixture (20 μL) was prepared using 10 μL of SYBR Premix Ex Taq (Takara, Japan), 1 μL of each forward and reverse primer (20 mM), 1 μL of DNA or cDNA template, and 7 μL of RNase-free water (Takara, Japan) according to the manufacturer's instructions. PCR program parameters are shown in Table S3, and all qPCR/RT-qPCR assays were carried out in triplicate. The copy number of DNA or cDNA was determined for each target gene based on a standard curve, with 10-fold dilutions of standards ranging from 10^7 to 10^1 copies. R^2 values were greater than 0.99. The specificity of targeted genes was confirmed by melting curve analyses. More details are presented in Table S4. The DNA copies of each gene were normalized to the content of total DNA, and the transcription level was calculated as cDNA copies/DNA copies.[36]

Biofilm Imaging and Antimony Reduction Production Characterization. At the end of S4, two ∼3-cm-long coupon fibers were cut off for scanning electron microscopy (SEM, Zeiss Sigma 300, German) and transmission electron microscopy (TEM, JEOL JEM 2100F, Japan) equipped with energy dispersive X-ray spectroscopy (EDS, Bruker Quad 5040, Germany).

Twenty main-column fibers were washed using deionized water, 100% acetone, and deionized water in sequence by centrifuging them three times at 10,000 *g* for 10 min for each solvent. The fibers were then desiccated in a freeze-dryer (FD-1A-50, BILON, China) to recover the antimony-reduction product, as described by Abin et al. and Lai et al.[11,31] X-ray photoelectron spectroscopy (XPS) was applied to analyze the valence state of reduction production through a Thermo Scientific K-Alpha (ThermoFisher, USA).

RESULTS AND DISCUSSION

Sb(V) Reduction in the H_2-MBfR. Figure 1A shows the influent and effluent concentrations of Sb(V) and Sb(III)

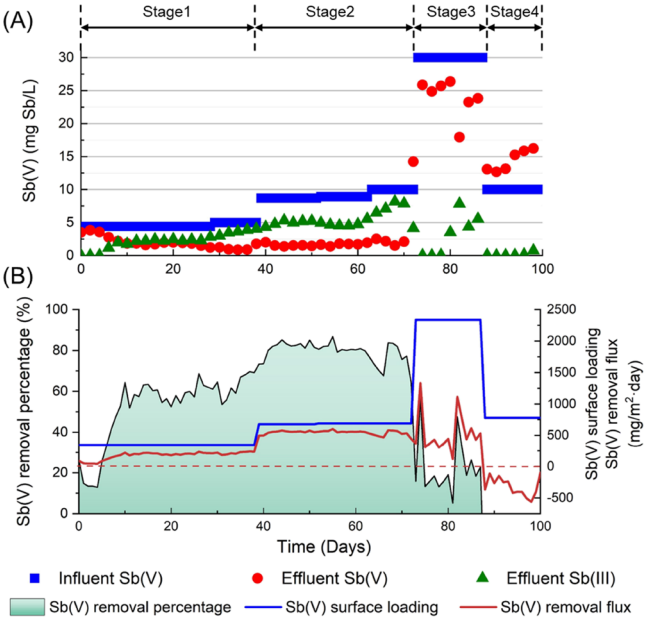

Figure 1. Sb(V)-reduction for all four stages of H_2-MBfR operation. Effluent concentrations are the average of two consecutive days and are after filtration.

during the entire operation of the H_2-MBfR. Figure 1B summarizes the Sb(V)-removal fluxes, surface loadings, and percentage removals. Table 1 summarizes the average steady-state fluxes of Sb(V) and H_2 during S1 to S4. It points out that the H_2-delivery capacity was greater than the H_2 flux for all stages.

After a 5-day start-up phase, S1's reduction percentage increased from ∼15 to ∼60% over the next 5 days and stabilized at ∼66%, which gave an average Sb(V)-reduction flux of 0.23 g/m^2 day at the end of S1. In S2 (Days 39−72), the removal percentage increased to ∼80% despite a doubling of the Sb(V) surface loading, and the Sb(V)-removal flux averaged 0.57 g/m^2 day at the steady state. The gradual increase of effluent Sb(III) in S1 and S2 confirmed that Sb(V) was being reduced.

The influent Sb(V) concentration was tripled, to 30 mg/L, in S3 to create stress from a high surface loading, although the H_2 demand did not exceed the H_2-supply capacity. The Sb(V) reduction flux reached its maximum value, 1.3 g/m^2 day on the first day (Day 74), but then dropped dramatically: the average reduction flux was 0.46 g/m^2 day by the end of S3, a value less

https://doi.org/10.1021/acs.est.2c04939
Environ. Sci. Technol. 2022, 56, 14808−14816

Table 1. Average Acceptor and Donor Fluxes for Each Stage of MBfR Operation

	surface loading $Sb(OH)_6^-$		actual $Sb(OH)_6^-$ flux		actual H_2 flux	theoretical maximum H_2 flux
stage	g Sb/m^2 d	e$^-$ eq/m^2 d	g Sb/m^2 d	e$^-$ eq/m^2 d	e$^-$ eq/m^2 d	e$^-$ eq/m^2 d
1	0.39	0.011	0.23	0.006	0.018	0.366
2	0.78	0.021	0.57	0.016	0.028	0.366
3	2.33	0.064	0.46	0.012	0.024	0.366
4	0.78	0.021	−0.32	−0.009	0.003	0.366

than that in S2. Likewise, the effluent Sb(III) concentration declined, averaging only 0.06 mg/L, equivalent to only 3% of the Sb(V)-removal flux, which means 97% of the Sb(III) formed by Sb(V) reduction (0.34 g/m^2 day) was retained by the biofilm.

The influent concentration of Sb(V) was returned to 10 mg/L in S4 (Days 88−100). Different from the ∼80% removal rate of S2, the effluent Sb(V) was higher than the influent Sb(V) during S4. This reveals that the Sb(V)-reducing microorganism may have been killed or lost due to the high Sb(V) concentration in S3 because MBfR performance failed to recover in 14 days.

The negative Sb(V) flux in S4 suggests that solid-phase Sb(III) retained in the biofilm was being oxidized in S4. Sb(III) oxidation requires that an electron acceptor be reduced. The only input acceptor was dissolved oxygen (DO). The flux of input DO was 0.078 g O_2/m^2 d by eq 2, which equals a 0.012 e$^-$ eq/m^2 d H_2 flux according to eq 4. Converting to an electron-equivalent flux, 0.078 g O_2/m^2 d could oxidize up to 0.46 g Sb/m^2 d in theory. Table 1 shows an observed Sb(III) oxidation flux of 0.32 g Sb/m^2 d, which means that Sb(III) oxidation to form Sb(V) was possible in terms of electron balance, but what is the terminal electron acceptor may need further study.

Sb mass balance during the operating stages was calculated; the sum of the effluent Sb(V), Sb(III), the accumulation Sb(III), and the Sb(V) removal percentage of every stage was presented in Figure S2. The ratio of the sum of effluent Sb(III) to the accumulation Sb(III) of S1−S3 is 7.97, 3.13, and 0.95. It means that the proportion of accumulation Sb(III) keeps increasing.

Biofilm Morphology and Product Characterization. Figure 2 characterizes the morphology of the biofilm and inorganic solids. SEM (Figure 2A, B) reveals that the biofilm contained bacilli and crystals having a cubic or orthorhombic shape. TEM (Figure 2C, D) shows black precipitates deposited in the biofilm (locations P_1) and inside one cell (location P_2). Vacuoles appeared in some bacilli after 100 days of Sb exposure (Figure 2C, D). EDS patterns (Figure S3A, B) targeting locations P_1 and P_2 in Figure 2D show that Sb was the main metal element in the precipitates. (Cu, Os, Pb, Bi, and U were introduced during sample pretreatment). XPS patterns comparing standard air-exposed Sb_2Te_3 (Figure 2E) and precipitates in biofilm (Figure 2F) show that Sb(III) was the predominant valence state for the Sb precipitates. Comparing standard Sb_2O_3 (Figure 2G) and precipitates in the biofilm (Figure 2F) shows that the Sb(III) peak binding energy was 529.9 eV, the same as that for standard Sb_2O_3, indicating that the reduction product precipitated in the biofilm was Sb_2O_3. Thus, Figure 2 documents that influent Sb(V) was reduced to Sb(III), which accumulated mostly extracellularly, but also intracellularly, although some Sb(III) remained soluble and appeared in the effluent (Figure 1). The

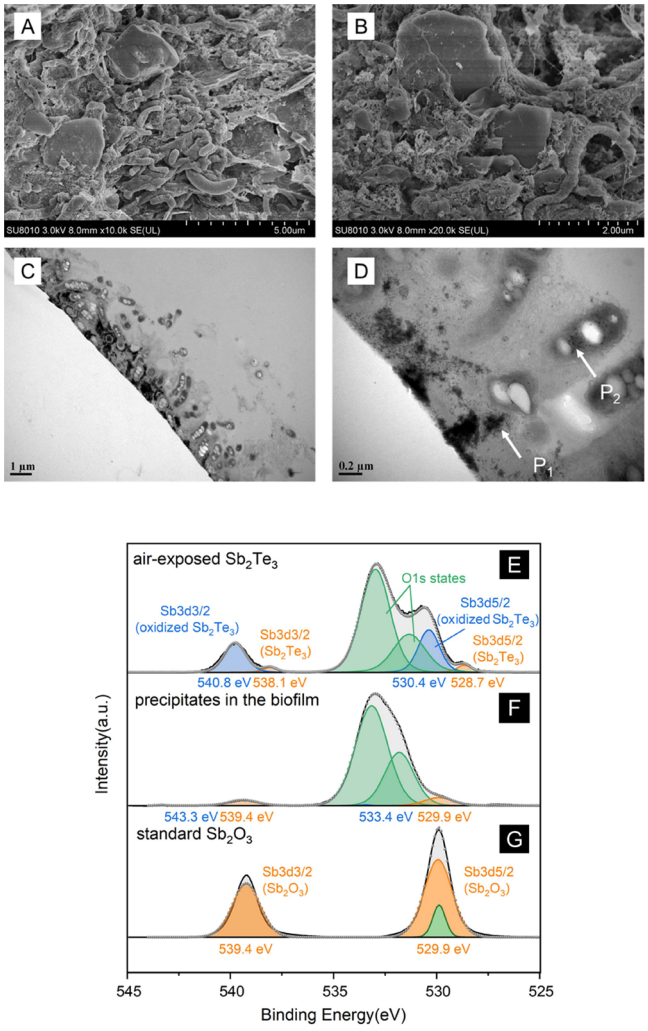

Figure 2. SEM was observed at 10,000-× (A) and 20,000-× (B) magnification. TEM was observed at 12,000-× (C) and 60,000-× (D) magnification. XPS of air-exposed Sb_2Te_3 (E), precipitates in the biofilm (F) and standard Sb_2O_3 (G).

fact that Sb(III) appeared outside and inside the cells suggests the possibility of two Sb(V)-reduction pathways.

Biofilm-Community Structure and Function. *Biofilm-Community Structure.* Figure 3 shows a heatmap of the cluster analysis of the microbial communities' phylogenetic structures at the genus level for S1−S4; it conveys the abundance of individual genus in every stage. Figure S4A presents the proportion of individual genera and the dominant genus in every stage. According to the genera-clustering tree, the genera could be divided into three groups: DSbRB (Dissimilatory Sb-reduction bacteria), which averaged about 63% from S1−4; SbRB (Sb-resistant bacteria), which on average occupied about 20% from S1−4; and DIRB

https://doi.org/10.1021/acs.est.2c04939
Environ. Sci. Technol. 2022, 56, 14808−14816

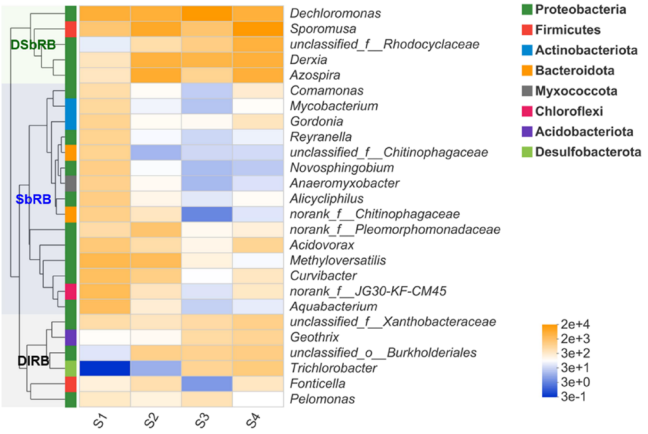

Figure 3. Heatmap of bacterial genera that occupied ≥1% of all sequences with all stages. The horizontal and vertical axes are stages and genera, respectively. The abundance of different species in the sample is displayed through the color gradient in the color column on the right side of the figure; its units are OTUs.

(Dissimilatory iron-reducing bacteria), which averaged about 6% from S1−4), as shown in Figure S4B.

Most of the genera in the DSbRB group (*Sporomusa*, *Derxia*, and *Azospira*) increased in S2 (along with the increase of influent Sb(V)), decreased in S3 due to the Sb(V) stress, and recovered in S4. One exception was unclassified_f_*Rhodocyclaceae*, which also increased in S3. Another exception was *Dechloromonas*, which decreased slightly in S2, but increased in S3. *Dechloromonas*,[37] *Sporomusa*,[38] unclassified_f_*Rhodocyclaceae*,[39] *Derxia*,[40] *and Azospira*[41] are identified as hydrogen-oxidizing DSbRB that have an *arrA* gene; additional details about the DSbRB are presented in the Supporting Information. In general, the change in major abundance of autotrophic DSbRB was positive relative to the influent Sb(V) concentration ($\rho > 0.3$, detailed in Table S5), indicating that DSbRB have a dissimilation Sb(V) respiration capacity using Sb(V) as an energy source.

Genera in the SbRB group were negatively correlated with the influent Sb(V) concentration over the operating stages ($\rho < -0.6$, detailed in Table S5), although norank_f_*Plemorphomonadaceae* and *Methyloversatilis* increased in S2. *Comamonas*,[42] *Mycobacterium*,[43] *Gordonia*,[44] *Reyranella*,[45] *Novosphingobium*,[46] *Anaeromyxobacter*,[47] *Acidovorax*,[48] *Methyloversatilis*,[49] *Curvibacter*,[50] and *Aquabacterium*[50] are known to possess genes associated with arsenic-resistance by its reduction, suggesting the potential to reduce Sb(V) using the arsenic-resistance pathway as a Sb-resistance strategy. Also, these genera were identified as heterotrophs,[51−59] which would account for the negative spearman correlation coefficient; although SbRB has an advantage in Sb resistance and appears more diverse, they could not get energy from this resistance pathway. In summary, although SbRB were negatively correlated to the influent Sb(V), they appeared to be more diverse and still occupied 19.6% in average (Figure S4B). Therefore, they were important in the biofilm community.

Within the DIRB group, unclassified_f_ *Xanthobacteraceae*,[60,61] *Geothrix*,[62,63] *Trichlorobacter*,[64,65] and *Fonticella*[66] are dissimilatory iron-reducing autotrophs. In general, the most genus-level abundance within this group was positively correlated with the influent Sb(V) concentration ($\rho > 0.3$, except *Fonticella*, detailed in Table S5). However, there was no Fe(III) in influent. The likely explanation for the sustained presence of DIRB is that they could carry out dissimilatory Sb(V) reduction. We propose in Figure S5 how Fe(III)-reducing bacteria are able to do dissimilatory Sb(V) reduction via their pathway for normal Fe(III) reduction.[67]

Biofilm-Community Function. Figure 4 shows the DNA abundances and RNA transcription levels for *arrA* and *arsC*

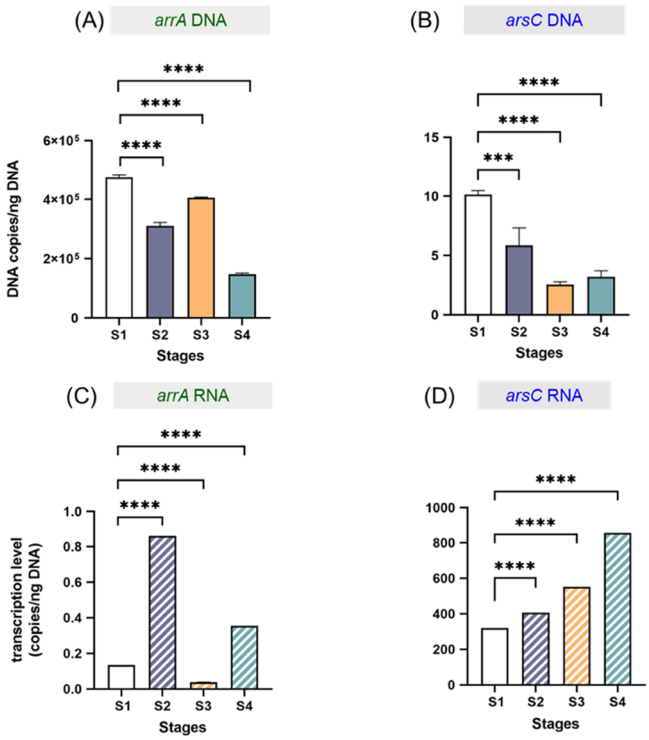

Figure 4. DNA abundances and RNA transcription levels of *arrA* and *arsC* genes during the entire operating period, based on the mean values from three replicate qPCR/RT-qPCR reactions. DNA abundances were normalized to the total-DNA concentration. Transcription levels were calculated by the odd ratios of cDNA copy numbers compared to total-DNA abundance.

genes during all operating stages. From S1 to S2, as the Sb(V)-removal flux increased (Figure 1B), both transcription levels became higher, although the increase was more dramatic for *arrA*. From S2 to S3, when the biofilm was stressed and the Sb(V)-reduction flux declined, the *arrA*-transcription level decreased dramatically, even though its DNA copies increased. In contrast, the expression level of *arsC* increased further, despite a drop in its DNA copies. The *arrA* DNA copies continued to decline in S4, and its transcription level also failed to recover. While its DNA copies did not change in S4, *arsC*'s transcription level increased greatly in S4. In general, the *arsC* DNA copies were negatively correlated with the influent Sb(V) (Figure 4B), presenting a similar change to the SbRB with the influent, but the *arsC* RNA copies increased over the stages (Figure 4D). The increasing transcriptional responses suggest the involvement in Sb(V) reduction similar to that in As(V) reduction, where ArsC is responsible for cytoplasmic Sb(V) reduction.

Illumina MiSeq sequencing targeting the *arrA* and *arsC* genes was employed to identify genera possessing these functional genes. The results, in Table S6, indicate that *Dechloromonas*, *unclassified_f_Rhodocyckaceae*, *Azospira*, *Methyloversatilis*, *Alicycliphilus*, *Acidovorax*, and *Aquabacterium*

https://doi.org/10.1021/acs.est.2c04939
Environ. Sci. Technol. 2022, 56, 14808−14816

possessed the *arrA* gene, where *Dechloromonas* and *Azospira* belong to DSbRB, while *Mycobacterium*, *Gordonia*, *Aquabacterium*, *Alicycliphilus*, *Azospira*, and *unclassified_f_Rhodocyckaceae* possessed the *arsC* gene, where all of them belong to SbRB except *Azospira* and *unclassified_f_Rhodocyckaceae*.

Taken together, the results in Figures 1, 2, and S2 and the results in Figure 4 point to respiratory reduction of Sb(V), mediated by ArrA, as the predominant mechanism in nonstress conditions (S1 and S2). However, imposition of Sb(V) stress in S3 shifted the mechanism toward detoxification mediated by ArsC, in which Sb(V) taken up by the microorganisms was reduced to Sb(III) and then accumulated inside the cell. The specific process about the derivation was presented in Section S11. **Detailed derivation process of the predominant mechanism.**

Antimony Metabolism Mechanisms. Dissimilatory antimonate reduction mediated by ArrAB and cytoplasmic antimonate reduction mediated by ArsC coexisted in the H_2-based MBfR. Figure 5 summarizes the likely Sb(V) reduction pathways based on our results.

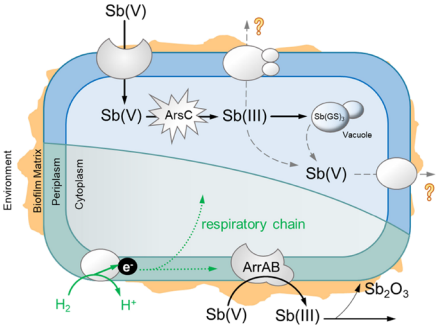

Figure 5. Schematic representation of the likely antimony-metabolism pathway. Solid line (—) indicates a pathway shown by our research here. Dashed line (---) signifies that the pathway might exist, which is reported in previously published work. Dotted line (···) indicates the respiratory chain that transports the electrons.

Dissimilatory Sb(V) reduction occurred on the outside of the bacterium's periplasm, mediated by ArrAB. Some of the produced Sb(III) was discharged in the effluent, but the other portion was hydrolyzed and retained in the biofilm as Sb_2O_3 solids. The dissimilatory antimonate-reduction pathway was stable during long-term continuous operation, and it enabled Sb(V) dissimilatory of DSbRB using hydrogen as the electron donor.

When Sb(V) was transported inside the cells, it could be reduced to Sb(III) by ArsC in the cell's cytoplasm. Sb(III) was sequestrated into a vacuole as the glutathione conjugate $Sb(GS)_3$. This is an antimony-resistance detoxification mechanism in SbRM and becomes predominant in stress conditions. However, the excess Sb(III) accumulation might disrupt the redox balance and lead an oxidation of Sb(III).[68] Therefore, the Sb(V) loading should be controlled to avoid cytoplasm Sb(V) reduction lead the route and make the dissimilatory in main route.

ENVIRONMENTAL IMPLICATIONS

A continuous-flow H_2-MBfR achieved Sb(V) bioreduction to Sb(III), which could form Sb_2O_3 precipitates that were retained in the biofilm. Long-term stable performance demonstrated that the H_2-MBfR is promising for Sb bioremediation, as long as too much stress from Sb(V) was avoided. Too-high Sb(V) loading caused a loss of Sb(V) removal flux that was not regained when the stress was lowered.

The main route for Sb(V) reduction in nonstress conditions was respiration-catalyzed by ArrA. However, Sb(V) stress led to increased importance of an intracellular reduction pathway catalyzed by ArsC, and Sb(V) stress led to deteriorated performance by the H_2-MBfR. By illuminating the roles of dissimilatory and cytoplasmic Sb(V) reduction in the H_2-MBfR, this study opens the door for using the H_2-MBfR as a Sb(V)-bioremediation technology, and it underscores that the Sb(V) loading should be controlled to avoid Sb stress that triggers cytoplasmic Sb(V) reduction as a resistance mechanism. For further research, we supposed the interactions of the metabolite of biofilms, the other common coexisting ions such as nitrate, sulfate, and ferric ions could be studied to enhance the understanding of the mechanism of Sb metabolism.

ASSOCIATED CONTENT

Supporting Information

The Supporting Information is available free of charge at https://pubs.acs.org/doi/10.1021/acs.est.2c04939.

Configuration of the MBfR system; Sb mass balance during the operating stages; EDS patterns of the precipitates; percentage of community and group abundance on the genus level; hypothesized scheme of Sb(V) reduction by DIRB; physical parameters of the MBfR; Spearman correlation of influent Sb(V) and genus abundance; identification of genera possessing target functional genes; compositions of the stock solutions (per liter of deionized H_2O); and detailed derivation process of the predominant mechanism (PDF)

AUTHOR INFORMATION

Corresponding Author

Siqing Xia − *State Key Laboratory of Pollution Control and Resource Reuse, College of Environmental Science and Engineering, Tongji University, Shanghai 200092, China; Shanghai Institute of Pollution Control and Ecological Security, Shanghai 200092, China;* orcid.org/0000-0002-5613-2681; Email: siqingxia@gmail.com

Authors

Jingzhou Zhou − *State Key Laboratory of Pollution Control and Resource Reuse, College of Environmental Science and Engineering, Tongji University, Shanghai 200092, China; Shanghai Institute of Pollution Control and Ecological Security, Shanghai 200092, China*

Chengyang Wu − *State Key Laboratory of Pollution Control and Resource Reuse, College of Environmental Science and Engineering, Tongji University, Shanghai 200092, China; Shanghai Institute of Pollution Control and Ecological Security, Shanghai 200092, China*

Si Pang − *State Key Laboratory of Pollution Control and Resource Reuse, College of Environmental Science and Engineering, Tongji University, Shanghai 200092, China; Shanghai Institute of Pollution Control and Ecological Security, Shanghai 200092, China*

Lin Yang − *State Key Laboratory of Pollution Control and Resource Reuse, College of Environmental Science and*

Engineering, Tongji University, Shanghai 200092, China; Shanghai Institute of Pollution Control and Ecological Security, Shanghai 200092, China

Mengying Yao − *State Key Laboratory of Pollution Control and Resource Reuse, College of Environmental Science and Engineering, Tongji University, Shanghai 200092, China; Shanghai Institute of Pollution Control and Ecological Security, Shanghai 200092, China*

Xiaodi Li − *State Key Laboratory of Pollution Control and Resource Reuse, College of Environmental Science and Engineering, Tongji University, Shanghai 200092, China; Shanghai Institute of Pollution Control and Ecological Security, Shanghai 200092, China*

Bruce E. Rittmann − *Biodesign Swette Center for Environmental Biotechnology, Arizona State University, Tempe, Arizona 85287-5701, United States;* orcid.org/0000-0002-3678-149X

Complete contact information is available at: https://pubs.acs.org/10.1021/acs.est.2c04939

Notes

The authors declare no competing financial interest.

■ ACKNOWLEDGMENTS

This work is supported by the National Key Project of Research and Development Plan of China (Grant No. 2021YFC3201300) and Shanghai Leading Talent Project (Grant No. 070).

■ REFERENCES

(1) Scheinost, A. C.; Rossberg, A.; Vantelon, D.; Xifra, I.; Kretzschmar, R.; Leuz, A.-K.; Funke, H.; Johnson, C. A. Quantitative Antimony Speciation in Shooting-Range Soils by EXAFS Spectroscopy. *Geochim. Cosmochim. Acta* **2006**, *70*, 3299−3312.

(2) *Mineral Commodity Summaries 2021*; Mineral Commodity Summaries; USGS Unnumbered Series; U.S. Geological Survey: Reston, VA, 2021; 200.

(3) He, M.; Wang, N.; Long, X.; Zhang, C.; Ma, C.; Zhong, Q.; Wang, A.; Wang, Y.; Pervaiz, A.; Shan, J. Antimony Speciation in the Environment: Recent Advances in Understanding the Biogeochemical Processes and Ecological Effects. *J. Environ. Sci.* **2019**, *75*, 14−39.

(4) Filella, M.; Belzile, N.; Chen, Y.-W. Antimony in the Environment: A Review Focused on Natural Waters: I. Occurrence. *Earth Sci. Rev.* **2002**, *57*, 125−176.

(5) Filella, M.; Belzile, N.; Chen, Y.-W. Antimony in the Environment: A Review Focused on Natural Waters: II. Relevant Solution Chemistry. *Earth Sci. Rev.* **2002**, *59*, 265−285.

(6) Zotov, A. V.; Shikina, N. D.; Akinfiev, N. N. Thermodynamic Properties of the Sb(III) Hydroxide Complex Sb(OH)3(Aq) at Hydrothermal Conditions. *Geochim. Cosmochim. Acta* **2003**, *67*, 1821−1836.

(7) Lai, C.-Y.; Wen, L.-L.; Zhang, Y.; Luo, S.-S.; Wang, Q.-Y.; Luo, Y.-H.; Chen, R.; Yang, X.; Rittmann, B. E.; Zhao, H.-P. Autotrophic Antimonate Bio-Reduction Using Hydrogen as the Electron Donor. *Water Res.* **2016**, *88*, 467−474.

(8) Liu, F.; Le, X. C.; McKnight-Whitford, A.; Xia, Y.; Wu, F.; Elswick, E.; Johnson, C. C.; Zhu, C. Antimony Speciation and Contamination of Waters in the Xikuangshan Antimony Mining and Smelting Area, China. *Environ. Geochem. Health* **2010**, *32*, 401−413.

(9) Wilson, S. C.; Lockwood, P. V.; Ashley, P. M.; Tighe, M. The Chemistry and Behaviour of Antimony in the Soil Environment with Comparisons to Arsenic: A Critical Review. *Environ. Pollut.* **2010**, *158*, 1169−1181.

(10) Kulp, T. R.; Miller, L. G.; Braiotta, F.; Webb, S. M.; Kocar, B. D.; Blum, J. S.; Oremland, R. S. Microbiological Reduction of Sb(V) in Anoxic Freshwater Sediments. *Environ. Sci. Technol.* **2014**, *48*, 218−226.

(11) Abin, C. A.; Hollibaugh, J. T. Dissimilatory Antimonate Reduction and Production of Antimony Trioxide Microcrystals by a Novel Microorganism. *Environ. Sci. Technol.* **2014**, *48*, 681−688.

(12) Ontiveros-Valencia, A.; Zhou, C.; Zhao, H.-P.; Krajmalnik-Brown, R.; Tang, Y.; Rittmann, B. E. Managing Microbial Communities in Membrane Biofilm Reactors. *Appl. Microbiol. Biotechnol.* **2018**, *102*, 9003−9014.

(13) Zhou, C.; Ontiveros-Valencia, A.; Nerenberg, R.; Tang, Y.; Friese, D.; Krajmalnik-Brown, R.; Rittmann, B. E. Hydrogenotrophic Microbial Reduction of Oxyanions With the Membrane Biofilm Reactor. *Front. Microbiol.* **2019**, *9*, 3268.

(14) Rittmann, B. E.; McCarty, P. L.*Environmental Biotechnology: Principles and Applications*; 2nd ed; McGraw-Hill Book Co: New York, 2014.

(15) Long, M.; Long, X.; Zheng, C.-W.; Luo, Y.-H.; Zhou, C.; Rittmann, B. E. Para-Chlorophenol (4-CP) Removal by a Palladium-Coated Biofilm: Coupling Catalytic Dechlorination and Microbial Mineralization via Denitrification. *Environ. Sci. Technol.* **2021**, *55*, 6309−6319.

(16) Wu, C.; Zhou, L.; Zhou, C.; Zhou, Y.; Xia, S.; Rittmann, B. E. Co-Removal of 2,4-Dichlorophenol and Nitrate Using a Palladized Biofilm: Denitrification-Promoted Microbial Mineralization Following Catalytic Dechlorination. *J. Hazard. Mater.* **2022**, *422*, No. 126916.

(17) Li, Z.; Ren, L.; Qiao, Y.; Li, X.; Zheng, J.; Ma, J.; Wang, Z. Recent Advances in Membrane Biofilm Reactor for Micropollutants Removal: Fundamentals Performance and Microbial Communities. *Bioresour. Technol.* **2022**, *343*, No. 126139.

(18) Zhao, H.-P.; Van Ginkel, S.; Tang, Y.; Kang, D.-W.; Rittmann, B.; Krajmalnik-Brown, R. Interactions between Perchlorate and Nitrate Reductions in the Biofilm of a Hydrogen-Based Membrane Biofilm Reactor. *Environ. Sci. Technol.* **2011**, *45*, 10155−10162.

(19) Li, J.; Wang, Q.; Oremland, R. S.; Kulp, T. R.; Rensing, C.; Wang, G. Microbial Antimony Biogeochemistry: Enzymes, Regulation, and Related Metabolic Pathways. *Appl. Environ. Microbiol.* **2016**, *82*, 5482−5495.

(20) Li, J.; Wang, Q.; Li, M.; Yang, B.; Shi, M.; Guo, W.; McDermott, T. R.; Rensing, C.; Wang, G. Proteomics and Genetics for Identification of a Bacterial Antimonite Oxidase in Agrobacterium Tumefaciens. *Environ. Sci. Technol.* **2015**, *49*, 5980−5989.

(21) Molecular Analysis of an ATP-Dependent Anion Pump. *Philos. Trans. R. Soc. Lond. B Biol. Sci.***1990**, *326* (), 455−463, DOI: 10.1098/rstb.1990.0024.

(22) Ruan, X.; Bhattacharjee, H.; Rosen, B. P. Characterization of the Metalloactivation Domain of an Arsenite/Antimonite Resistance Pump: Metalloactivation Domain of ArsA. *Mol. Microbiol.* **2008**, *67*, 392−402.

(23) Kruger, M. C.; Bertin, P. N.; Heipieper, H. J.; Arsène-Ploetze, F. Bacterial Metabolism of Environmental Arsenic—Mechanisms and Biotechnological Applications. *Appl. Microbiol. Biotechnol.* **2013**, *97*, 3827−3841.

(24) Wang, L.; Ye, L.; Jing, C. Genetic Identification of Antimonate Respiratory Reductase in *Shewanella* Sp. ANA-3. *Environ. Sci. Technol.* **2020**, *54*, 14107−14113.

(25) Li, J.; Yang, B.; Shi, M.; Yuan, K.; Guo, W.; Li, M.; Wang, G. Effects upon Metabolic Pathways and Energy Production by Sb(III) and As(III)/Sb(III)-Oxidase Gene AioA in Agrobacterium Tumefaciens GW4. *PLoS One* **2017**, *12*, No. e0172823.

(26) Wysocki, R.; Chéry, C. C.; Wawrzycka, D.; Van Hulle, M.; Cornelis, R.; Thevelein, J. M.; Tamás, M. J. The Glycerol Channel Fps1p Mediates the Uptake of Arsenite and Antimonite in Saccharomyces Cerevisiae. *Mol. Microbiol.* **2001**, *40*, 1391−1401.

(27) Gu, J.; Yao, J.; Duran, R.; Sunahara, G. Comprehensive Genomic and Proteomic Profiling Reveal Acinetobacter Johnsonii JH7 Responses to Sb(III) Toxicity. *Sci. Total Environ.* **2020**, *748*, No. 141174.

(28) Wu, C.; Zhou, L.; Zhou, Y.; Zhou, C.; Xia, S.; Rittmann, B. E. Dechlorination of 2,4-Dichlorophenol in a Hydrogen-Based Mem-

brane Palladium-Film Reactor: Performance, Mechanisms, and Model Development. *Water Res.* **2021**, *188*, No. 116465.
(29) Tang, Y.; Zhou, C.; Van Ginkel, S. W.; Ontiveros-Valencia, A.; Shin, J.; Rittmann, B. E. Hydrogen Permeability of the Hollow Fibers Used in H2-Based Membrane Biofilm Reactors. *J. Membr. Sci.* **2012**, *407-408*, 176−183.
(30) Wu, C.; Zhou, L.; Zhou, C.; Zhou, Y.; Zhou, J.; Xia, S.; Rittmann, B. E. A Kinetic Model for 2,4-Dichlorophenol Adsorption and Hydrodechlorination over a Palladized Biofilm. *Water Res.* **2022**, *214*, No. 118201.
(31) Lai, C.-Y.; Dong, Q.-Y.; Rittmann, B. E.; Zhao, H.-P. Bioreduction of Antimonate by Anaerobic Methane Oxidation in a Membrane Biofilm Batch Reactor. *Environ. Sci. Technol.* **2018**, *52*, 8693−8700.
(32) Rittmann, B. E.; Mccarty, P. L.Environmental Biotechnology: Principles and Applications. *Environ. Biotechnol. Princ. Appl.*; McGraw-Hill Education, 2014, xiv.
(33) Muyzer, G.; de Waal, E. C.; Uitterlinden, A. G. Profiling of Complex Microbial Populations by Denaturing Gradient Gel Electrophoresis Analysis of Polymerase Chain Reaction-Amplified Genes Coding for 16S RRNA. *Appl. Environ. Microbiol.* **1993**, *59*, 695−700.
(34) Edgar, R. C. UPARSE: Highly Accurate OTU Sequences from Microbial Amplicon Reads. *Nat. Methods* **2013**, *10*, 996−998.
(35) Li, W.; Zhang, M.; Kang, D.; Chen, W.; Yu, T.; Xu, D.; Zeng, Z.; Li, Y.; Zheng, P. Mechanisms of Sulfur Selection and Sulfur Secretion in a Biological Sulfide Removal (BISURE) System. *Environ. Int.* **2020**, *137*, No. 105549.
(36) Lee, C.; Kim, J.; Shin, S. G.; Hwang, S. Absolute and Relative QPCR Quantification of Plasmid Copy Number in Escherichia Coli. *J. Biotechnol.* **2006**, *123*, 273−280.
(37) Shrout, J. D.; Scheetz, T. E.; Casavant, T. L.; Parkin, G. F. Isolation and Characterization of Autotrophic, Hydrogen-Utilizing, Perchlorate-Reducing Bacteria. *Appl. Microbiol. Biotechnol.* **2005**, *67*, 261−268.
(38) Möller, B.; Oßmer, R.; Howard, B. H.; Gottschalk, G.; Hippe, H. Sporomusa a New Genus of Gram-Negative Anaerobic Bacteria Including Sporomusa Sphaeroides Spec Nov. and Sporomusa Ovata Spec. Nov. *Arch. Microbiol.* **1984**, *139*, 388−396.
(39) Barbosa, R. G.; Sleutels, T.; Verstraete, W.; Boon, N. Hydrogen Oxidizing Bacteria Are Capable of Removing Orthophosphate to Ultra-Low Concentrations in a Fed Batch Reactor Configuration. *Bioresour. Technol.* **2020**, *311*, No. 123494.
(40) Gerstenberg, C.; Friedrich, B.; Schlegel, H. G. Physical Evidence for Plasmids in Autotrophic, Especially Hydrogen-Oxidizing Bacteria. *Arch. Microbiol.* **1982**, *133*, 90−96.
(41) Nam, J.-H.; Ventura, J.-R. S.; Yeom, I. T.; Lee, Y.; Jahng, D. A Novel Perchlorate- and Nitrate-Reducing Bacterium Azospira Sp. PMJ. *Appl. Microbiol. Biotechnol.* **2016**, *100*, 6055−6068.
(42) Zhang, Y.; Ma, Y.-F.; Qi, S.-W.; Meng, B.; Chaudhry, M. T.; Liu, S.-Q.; Liu, S.-J. Responses to Arsenate Stress by Comamonas Sp. Strain CNB-1 at Genetic and Proteomic Levels. *Microbiology* **2007**, *153*, 3713−3721.
(43) Chen, J.; Galván, A. E.; Nadar, V. S.; Yoshinaga, M.; Rosen, B. P. An ArsRC Fusion Protein Enhances Arsenate Sensing and Detoxification. *Environ. Microbiol.* **2022**, *24*, 1977−1987.
(44) Sowani, H.; Kulkarni, M.; Zinjarde, S. An Insight into the Ecology, Diversity and Adaptations of Gordonia Species. *Crit. Rev. Microbiol.* **2018**, *44*, 393−413.
(45) Chen, J.; Zhang, J.; Wu, Y.-F.; Zhao, F.-J.; Rosen, B. P. ArsV and ArsW Provide Synergistic Resistance to the Antibiotic Methylarsenite. *Environ. Microbiol.* **2021**, *23*, 7550−7562.
(46) Chen, W.-M.; Cai, C.-Y.; Sheu, D.-S.; Tsai, J.-M.; Sheu, S.-Y. Novosphingobium Ovatum Sp. Nov., Isolated from a Freshwater Mesocosm. *Int. J. Syst. Evol. Microbiol.* **2020**, *70*, 5243−5254.
(47) Tonomura, M.; Ehara, A.; Suzuki, H.; Amachi, S. Draft Genome Sequence of Anaeromyxobacter Sp. Strain PSR-1, an Arsenate-Respiring Bacterium Isolated from Arsenic-Contaminated Soil. *Genome Announc.* **2015**, *3*, e00472−e00415.
(48) Huang, Y.; Li, H.; Rensing, C.; Zhao, K.; Johnstone, L.; Wang, G. Genome Sequence of the Facultative Anaerobic Arsenite-Oxidizing and Nitrate-Reducing Bacterium Acidovorax Sp. Strain NO1. *J. Bacteriol.* **2012**, *194*, 1635−1636.
(49) Li, J.; Wang, Q.; Zhang, S.; Qin, D.; Wang, G. Phylogenetic and Genome Analyses of Antimony-Oxidizing Bacteria Isolated from Antimony Mined Soil. *Int. Biodeterior. Biodegrad.* **2013**, *76*, 76−80.
(50) Nabi, A.; Naeem, M.; Aftab, T.; Khan, M. M. A.; Ahmad, P. A Comprehensive Review of Adaptations in Plants under Arsenic Toxicity: Physiological Metabolic and Molecular Interventions. *Environ. Pollut.* **2021**, *290*, No. 118029.
(51) Etchebehere, C.; Errazquin, M. I.; Dabert, P.; Moletta, R.; Muxí, L. Comamonas Nitrativorans Sp. Nov., a Novel Denitrifier Isolated from a Denitrifying Reactor Treating Landfill Leachate. *Int. J. Syst. Evol. Microbiol.* **2001**, *51*, 977−983.
(52) Torvinen, E.; Suomalainen, S.; Lehtola, M. J.; Miettinen, I. T.; Zacheus, O.; Paulin, L.; Katila, M.-L.; Martikainen, P. J. Mycobacteria in Water and Loose Deposits of Drinking Water Distribution Systems in Finland. *Appl. Environ. Microbiol.* **2004**, *70*, 1973−1981.
(53) Carneiro Fidélis Silva, L.; Santiago Lima, H.; Antônio de Oliveira Mendes, T.; Sartoratto, A.; de Paula Sousa, M.; Suhett de Souza, R.; Oliveira de Paula, S.; Maia de Oliveira, V.; Canêdo da Silva, C. Heterotrophic Nitrifying/Aerobic Denitrifying Bacteria: Ammonium Removal under Different Physical-Chemical Conditions and Molecular Characterization. *J. Environ. Manage.* **2019**, *248*, No. 109294.
(54) Roy, D.; Lemay, J.-F.; Drogui, P.; Tyagi, R. D.; Landry, D.; Rahni, M. Identifying the Link between MBRs' Key Operating Parameters and Bacterial Community: A Step towards Optimized Leachate Treatment. *Water Res.* **2020**, *172*, No. 115509.
(55) Huang, G.; Huang, Y.; Hu, H.; Liu, F.; Zhang, Y.; Deng, R. Remediation of Nitrate−Nitrogen Contaminated Groundwater Using a Pilot-Scale Two-Layer Heterotrophic−Autotrophic Denitrification Permeable Reactive Barrier with Spongy Iron/Pine Bark. *Chemosphere* **2015**, *130*, 8−16.
(56) Saxena, G.; Hill, E. D.; Marzinelli, E. M.; Umashankar, S.; Wei, T. J.; Yissue, W. W.; Steinberg, P. D.; Rajal, V. B.; Kjelleberg, S.; Williams, R. B. H.; Wuertz, S.; Swarup, S. Integrative Systems Approach Reveals Dynamics of Microbiome-Metal-Ion Axis in Mesocosms Representing Tropical Urban Freshwater Canal Ecosystem. *bioRxiv* **2020**, *21*, 2020.09.21.306803.
(57) Zhang, L.; Zhang, C.; Hu, C.; Liu, H.; Bai, Y.; Qu, J. Sulfur-Based Mixotrophic Denitrification Corresponding to Different Electron Donors and Microbial Profiling in Anoxic Fluidized-Bed Membrane Bioreactors. *Water Res.* **2015**, *85*, 422−431.
(58) Wang, Y.; Bott, C.; Nerenberg, R. Sulfur-Based Denitrification: Effect of Biofilm Development on Denitrification Fluxes. *Water Res.* **2016**, *100*, 184−193.
(59) Sultana, M.; Mou, T. J.; Sanyal, S. K.; Diba, F.; Mahmud, Z. H.; Parvez, A. K.; Hossain, M. A. Investigation of Arsenotrophic Microbiome in Arsenic-Affected Bangladesh Groundwater. *Groundwater* **2017**, *55*, 736−746.
(60) Wang, X.; Teng, Y.; Ren, W.; Li, Y.; Yang, T.; Chen, Y.; Zhao, L.; Zhang, H.; Kuramae, E. E. Variations of Bacterial and Diazotrophic Community Assemblies throughout the Soil Profile in Distinct Paddy Soil Types and Their Contributions to Soil Functionality. *mSystems* **2022**, *7*, No. e0104721.
(61) Akinyede, R.; Taubert, M.; Schrumpf, M.; Trumbore, S.; Küsel, K. Rates of Dark CO2 Fixation Are Driven by Microbial Biomass in a Temperate Forest Soil. *Soil Biol. Biochem.* **2020**, *150*, No. 107950.
(62) Islam, F. S.; Boothman, C.; Gault, A. G.; Polya, D. A.; Lloyd, J. R. Potential Role of the Fe(III)-Reducing Bacteria *Geobacter* and *Geothrix* in Controlling Arsenic Solubility in Bengal Delta Sediments. *Mineral. Mag.* **2005**, *69*, 865−875.
(63) Zhang, L.; Song, Y.; Zuo, Y.; Huo, S.; Liang, C.; Hu, C. Integrated Sulfur- and Iron-Based Autotrophic Denitrification Process and Microbial Profiling in an Anoxic Fluidized-Bed Membrane Bioreactor. *Chemosphere* **2019**, *221*, 375−382.

(64) Nevin, K. P.; Holmes, D. E.; Woodard, T. L.; Covalla, S. F.; Lovley, D. R. Y. Reclassification of Trichlorobacter Thiogenes as Geobacter Thiogenes Comb. Nov. *Int. J. Syst. Evol. Microbiol.* **2007**, *57*, 463−466.
(65) Chen, G.-W.; Choi, S.-J.; Lee, T.-H.; Lee, G.-Y.; Cha, J.-H.; Kim, C.-W. Application of Biocathode in Microbial Fuel Cells: Cell Performance and Microbial Community. *Appl. Microbiol. Biotechnol.* **2008**, *79*, 379−388.
(66) Slobodkin, A.; Campbell, B.; Cary, S. C.; Bonch-Osmolovskaya, E.; Jeanthon, C. Evidence for the Presence of Thermophilic Fe(III)-Reducing Microorganisms in Deep-Sea Hydrothermal Vents at 13°N (East Pacific Rise). *FEMS Microbiol. Ecol.* **2001**, *36*, 235−243.
(67) Jiang, J.; Kappler, A. Kinetics of Microbial and Chemical Reduction of Humic Substances: Implications for Electron Shuttling. *Environ. Sci. Technol.* **2008**, *42*, 3563−3569.
(68) Deng, R.; Chen, Y.; Deng, X.; Huang, Z.; Zhou, S.; Ren, B.; Jin, G.; Hursthouse, A. A Critical Review of Resistance and Oxidation Mechanisms of Sb-Oxidizing Bacteria for the Bioremediation of Sb(III) Pollution. *Front. Microbiol.* **2021**, *12*, No. 738596.

https://doi.org/10.1021/acs.est.2c04939
Environ. Sci. Technol. 2022, 56, 14808−14816